CHROMATOR IS REQUIRED FOR PROPER MICROTUBULE SPINDLE FORMATION AND MITOSIS IN *DROSOPHILA*

Yun Ding[1], Changfu Yao[1], Mariana Lince-Faria[2], Uttama Rath[1], Weili Cai[1], Helder Maiato[2,3], Jack Girton[1], Kristen M. Johansen[1] and Jørgen Johansen[1]

[1]Department of Biochemistry, Biophysics, and Molecular Biology
Iowa State University
Ames, Iowa 50011

[2]Instituto de Biologia Molecular e Celular and [3]Laboratory for Cell and Molecular Biology, Faculdade de Medicina, Universidade do Porto, Rua do Campo Alegre 823, 4150-180 Porto, Portugal

Short title: *Chromator and spindle formation*

Key words: *Chromator, spindle-assembly checkpoint, mitosis, spindle matrix, Drosophila*

CORRESPONDENCE: Jorgen Johansen
Department of Biochemistry, Biophysics, and Molecular Biology
3156 Molecular Biology Building
Iowa State University
Ames, Iowa 50011
ph. (515) 294-2358; fax. (515) 294-4858;
E-mail: *jorgen@iastate.edu*

ABSTRACT

The chromodomain protein, Chromator, has been shown to have multiple functions that include regulation of chromatin structure as well as coordination of muscle remodeling during metamorphosis depending on the developmental context. In this study we show that mitotic neuroblasts from brain squash preparations from larvae heteroallelic for the two *Chromator* loss-of-function alleles *Chro*^{71} and *Chro*^{612} have severe microtubule spindle and chromosome segregation defects that were associated with a reduction in brain size. The microtubule spindles formed were incomplete, unfocused, and/or without clear spindle poles and at anaphase chromosomes were lagging and scattered. Time-lapse analysis of mitosis in S2 cells depleted of Chromator by RNAi treatment suggested that the lagging and scattered chromosome phenotypes were caused by incomplete alignment of chromosomes at the metaphase plate, possibly due to a defective spindle-assembly checkpoint, as well as of frayed and unstable microtubule spindles during anaphase. Expression of full-length Chromator transgenes under endogenous promoter control restored both microtubule spindle morphology as well as brain size strongly indicating that the observed mutant defects were directly attributable to lack of Chromator function.

INTRODUCTION

The chromodomain protein, Chromator, localizes to interband regions of *Drosophila* polytene chromosomes at interphase (Rath et al., 2004; Gortchakov et al., 2005) but redistributes during mitosis to form a molecular spindle matrix complex together with three other nuclear derived proteins Skeletor, Megator, and EAST (Walker et al., 2000; Rath et al., 2004; Qi et al., 2004; 2005). This complex forms a fusiform spindle structure that persists in the absence of polymerized tubulin and has been proposed based on theoretical considerations of the requirements for force production to help stabilize the microtubule spindle apparatus during mitosis (reviewed in Johansen and Johansen, 2007). Previously, it has been demonstrated that Chromator regulates chromatin structure and organization of polytene chromosomes at interphase (Rath et al., 2006) and biochemical evidence has suggested that it may play an additional role in transcriptional regulation through association with the male specific dosage compensation complex (Mendjan et al., 2006). Moreover, Wasser et al. (2007) showed that Chromator participates in the coordination of muscle remodeling during *Drosophila* metamorphosis. Thus, Chromator is likely to have multiple functions depending on the developmental context. Here we demonstrate the requirement for Chromator function for proper microtubule spindle formation and mitosis in *Drosophila* larval neuroblasts using two recently generated loss-of-function alleles, $Chro^{71}$ and $Chro^{612}$ (Rath et al., 2006). Our data show that neuroblasts from $Chro^{71}/Chro^{612}$ brain squash preparations have severe microtubule spindle and chromosome segregation defects that were associated with a developmental small brain phenotype. Time-lapse analysis of mitosis in S2 cells depleted of Chromator by RNAi treatment suggested that the chromosome segregation defects were the results of incomplete alignment of chromosomes at the metaphase plate, possibly due to a defective spindle-assembly checkpoint, as well as of frayed and unstable microtubule spindles during anaphase.

MATERIALS AND METHODS

Chromator constructs.

For NP-Chro, part of the *Chromator* genomic region containing 353 nucleotides of 5' upstream sequence from the starting ATG codon and the first three exons and introns was PCR amplified from Canton S. genomic sequence and fused with the remaining *Chromator* cDNA sequence using standard methods (Sambrook and Russell, 2001). The resulting full length Chromator coding sequence (1-926 aa) and its 5' regulatory elements was inserted into the pUASP vector (Rorth, 1998) with a C-terminal in frame GFP tag. In this process a NP-chro construct with a point mutation leading to a N^{41} to D^{41} amino acid change was also generated. For Chro-FL, *Chromator* full length cDNA sequence corresponding to residues 1-926 was inserted into the pUAST vector (Brand and Perrimon, 1993) with a C-terminal GFP tag. For Chro-NTD, cDNA sequence corresponding to Chromator N-terminal residues 1-346 was inserted into the pUASP vector (Rorth, 1998) with a C-terminal GFP tag. Three tandemly arrayed nuclear localization sequences (NLS) excised from the pECFP vector (Clontech) were added to the C-terminus. For Chro-CTD, cDNA sequence corresponding to the Chromator C-terminal residues 329-926 was inserted into the pUASP vector (Rorth, 1998) with a N-terminal GFP tag. Chro-CTD contains the endogenous NLS (Rath et al., 2004). The fidelity of the constructs was verified by sequencing at the Iowa State University DNA Facility.

Drosophila melanogaster stocks

Fly stocks were maintained according to standard protocols (Roberts, 1998). Canton S was used for wild-type preparations. The $JIL\text{-}1^{z2}$ null allele was described in Wang et al. (Wang et al., 2001) and in Zhang et al. (Zhang et al., 2003). The *Chro* mutant alleles $Chro^{71}$ and $Chro^{612}$ as well as the transheterozygous $Chro^{71}/Chro^{612}$ allelic combination were described in Rath et al. (2006). Chromator construct pUAST or pUASP transgenic lines were generated by standard P-element transformation (BestGene, Inc.), and expression of the transgenes was driven using the

nervous system specific *GAL4* driver *P{w[+mW.hs]=GawB}elav[C155]* (Bloomington Stock Center) introduced by standard genetic crosses or by the endogenous promoter. Expression levels of each of the Chromator constructs were monitored by immunoblot analysis as described below. Viability assays were performed as in Zhang et al. (2003). Balancer chromosomes and markers are described in Lindsley and Zimm, 1992.

Immunocytochemistry

Larval brain squashes were performed with minor modifications according to the protocol of Bonaccorsi et al., (2000). In brief, third instar larval brains were dissected in 0.7% physiological insect saline solution and rinsed in PBS. For antibody labelings the brains were fixed with 4% PFA for 30 min, postfixed for 3 min in 45% acetic acid, and subsequently gently squashed in 60% acetic acid. Squashed samples on the slides were washed in PBT (PBS containing 0.4% Triton X-100) three times (10 min each), then blocked for 1 hour in 1% NGS in PBT . Immunostaining of neuroblasts identified by their large size was performed by incubation with diluted primary antibody in PBS containing 0.4% Triton X-100, 0.1% sodium azide, and 1% normal goat serum for 1.5 h to overnight. Quantification of mutant spindle phenotypes in mitotic neuroblasts were based on data from at least 20 individual brain squash preparations. Standard polytene chromosome squash preparations were performed as in Kelley et al. (1999) using the 5 min fixation protocol and antibody labeling of these preparations was performed as described in Jin et al. (1999) and in Wang et al. (2001). Antibody labelings of 0–3 h embryos were performed as previously described (Johansen and Johansen, 2003). Immmunofluorescence microscopy in *Drosophila* S2 cells was performed as described in Maiato et al. (2006). Mad2 accumulation at the kinetochores was measured for individual kinetochores by quantification of the pixel gray levels of the focused z-plane within a region of interest (ROI). Background was measured outside the ROI and was subtracted to the measured fluorescent intensity inside the ROI. Results were normalized against a constitutive kinetochore marker Cid using a custom routine written in Matlab. Microtubule depolymerization in S2 cells was induced by colchicine at 30 μM for 18 h for the quantification of

mitotic index or immunofluorescence analysis of kinetochore proteins. Primary antibodies used include the Chromator specific mAbs 6H11 and 12H9 (Rath et al., 2004), Ncd pAb (the generous gift of Dr. Sharyn A. Endow, Duke University, Durham, NC), caspase 3 pAb (Epitomics), H3S10ph pAb (Upstate Inc.), anti-α-tubulin mAb (Sigma-Aldrich), Cid pAb (provided by Dr. S. Henikoff, Fred Hutchinson Cancer Research Center, Seattle, WA), Mad2 pAb (provided by Dr. C. Sunkel, Instituto de Biologia Molecular e Celular, Porto, Portugal), and anti-GFP pAb (Invitrogen). DNA was visualized by staining with Hoechst 33258 or DAPI (Molecular Probes) in PBS. The appropriate species- and isotype- specific Texas Red-, TRITC-, and FITC-conjugated secondary antibodies (Cappel/ICN, Southern Biotech) were used (1:200 dilution) to visualize primary antibody labeling. TUNEL assays of squashes from wt and $Chro^{71}/Chro^{612}$ mutant brains including DNase treated positive controls were performed using the DeadEnd™ Fluorometric TUNEL System kit from Promega according to the manufacturer's instructions. The final preparations were mounted in 90% glycerol containing 0.5% *n*-propyl gallate. The preparations were examined using epifluorescence optics on a Zeiss Axioskop microscope and images were captured and digitized using a high resolution Spot CCD camera. Images were imported into Photoshop where they were pseudocolored, image processed, and merged. In some images non-linear adjustments were made to the channel with Hoechst labeling for optimal visualization of chromosomes.

Immunoblot analysis

Protein extracts were prepared from brains dissected from third instar larvae (or in some experiments from whole larvae) homogenized in a buffer containing: 20 mM Tris-HCl pH8.0, 150 mM NaCl, 10 mM EDTA, 1 mM EGTA, 0.2% Triton X-100, 0.2% NP-40, 2 mM Na_3VO_4, 1 mM PMSF, 1.5 μg/ml aprotinin. Proteins were separated by SDS-PAGE according to standard procedures (Laemmli, 1970). Electroblot transfer was performed as in Towbin et al. (1979) with transfer buffer containing 20% methanol and in most cases including 0.04% SDS. For these

experiments we used the Bio-Rad Mini PROTEAN II system, electroblotting to 0.2 µm nitrocellulose, and using anti-mouse or anti-rabbit HRP-conjugated secondary antibody (Bio-Rad) (1:3000) for visualization of primary antibody. Antibody labeling was visualized using chemiluminescent detection methods (SuperSignal West Pico Chemiluminescent Substrate, Pierce). The immunoblots were digitized using a flatbed scanner (Epson Expression 1680).

Time-lapse microscopy and Chromator RNAi depletion in S2 cells

Time-lapse imaging of a full-length GFP-tagged Chromator construct (NP-Chro) in live syncytial embryos was performed using the Leica confocal TCS SP7 microscope system using a 488 nm laser line. The embryos were mounted on a coated coverslip in Voltalef oil and time-lapse images of z-stacks covering the depth of the mitotic apparatus were collected every 5 s.

The S2 cell line stably expressing GFP-α-tubulin and mCherry-Cid has been previously described (Lince-Faria et al., 2009) and was grown on concanavalin A coated coverslips in modified Rose chambers with Schneider´s medium (Sigma) containing 10% of FBS. Four dimensional data sets were collected at 25ºC with an Andor Revolution Spinning Disc confocal system (Andor) equipped with an Electron Multiplying CCD (EMCCD) iXonEM+ camera and a Yokogawa CSU-22 unit based on an Olympus IX81 inverted microscope. Two laser lines (488 and 561 nm) were used for near-simultaneous excitation of GFP and mCherry and the system was driven by Andor IQ software. Time-lapse imaging of z-stacks with 1 µm steps covering the entire volume of the mitotic apparatus were collected every 30 s. Depletion of Chromator by RNAi treatment was performed as previously described (Rath et al., 2004).

Analysis of gene expression by qRT-PCR

Total RNA was extracted from 12 pooled whole third instar larvae of each genotype (wild type, $Chro^{71}/Chro^{612}$ and $JIL\text{-}1^{z2}/JIL\text{-}1^{z2}$) using the MicroPoly(A)Purist Small-Scale mRNA Purification Kit (Ambion) following the manufacturer's instructions. cDNA derived from this RNA

using SuperScript II Reverse Transcriptase (Invitrogen) was used as template for quantitative real-time (qRT) PCR performed with the Stratagene Mx4000 real-time cycler. In addition, the PCR mixture contained Brilliant II SYBR Green QPCR Master Mix (Stratagene) as well as the corresponding primers: *rp49*, 5'-AACGTTTACAAATGTGTATTCCGACC-3' and 5'-ATGACCATCCGCCCAGCATACAGG-3'; *ncd*, 5'GCCAAGAACAACAAGAACGACATCTACG-3' and 5'-AAACTGCCGCTGTTGTTGCTCTGTGTG-3'. Cycling parameters were 10 min at 95°C, followed by 40 cycles of 30 s at 95°C, 60 s at 60°C, and 30 s at 72°C. Fluorescence intensities were plotted against the number of cycles using an algorithm provided by Stratagene. mRNA levels were quantified using a calibration curve based on dilution of concentrated cDNA. mRNA values from the larvae were normalized to that of *rp49*.

Imaging of whole larval brains

Wild type and $Chro^{71}/Chro^{612}$ mutant brains from crawling third instar larvae were dissected in physiological saline (110 mM NaCl, 4 mM KCl, 2 mM $CaCl_2$, 10 mM glucose, 10 mM HEPES, pH. 7.4) under an Olympus dissection microscope and images of the live unfixed brains were taken with a Spot CCD camera.

RESULTS

In order to be able to study the effect of impaired Chromator function on mitosis in larval neuroblasts we have recently generated two hypomorphic loss-of-function *Chromator* alleles, *Chro*^{71} and *Chro*^{612} (Rath et al., 2006). The *Chro*^{71} allele is comprised of a G to A nucleotide change at nucleotide position 402 of the *Chromator* transcribed sequence that introduces a premature stop codon resulting in a truncated 71 amino acid protein (Rath et al., 2006). The truncated NH_2-terminal fragment does not contain the chromodomain and *Chro*^{71} is likely to act as a null allele. *Chro*^{71} is homozygous embryonic lethal with no first instar larval escapers. The *Chro*^{612} allele consists of a C to T nucleotide change at nucleotide position 2024 that introduces a premature stop codon resulting in a truncated 612 amino acid protein that retains the chromodomain (Rath et al., 2006) but is missing parts of the COOH-terminal domain important for spindle localization (Rath et al., 2004) and for interactions with Skeletor (Rath et al., 2004) and EAST (Wasser et al., 2007). *Chro*^{71}*/Chro*^{612} transheterozygotes survive to third instar larval stages although no larvae have been observed to pupate. As illustrated in Fig. 1 mitotic neuroblasts from *Chro*^{71}*/Chro*^{612} brain squash preparations labeled with tubulin and histone H3S10ph antibody (as a marker for dividing cells) in contrast to wild type neuroblasts (Fig. 1A) have severe spindle and chromosome segregation defects (Fig. 1B). The microtubule spindles were incomplete (Fig. 1B1), unfocused (Fig. 1B2), and/or without clear spindle poles (Fig. 1B3-6). At anaphase chromosomes were lagging and scattered indicating impaired spindle function (Fig. 1B5-6). This phenotype is similar to that obtained by RNAi depletion of Chromator in S2 cells (Rath et al., 2004). We quantified these differences by determining the frequency of such phenotypes in *Chro*^{71}*/Chro*^{612} mutant brains and compared it to wild-type (Fig. 1C). In mutant brains (n=76) 537 out of 595 (90.3%) neuroblasts examined had such phenotypes versus only 30 out of 364 (8.2%) neuroblasts in control brains (n=22). This difference is statistically significant on the $p<0.001$ level (χ^2-test). Furthermore, the mitotic index in *Chromator* mutant brains was significantly reduced

($p<0.001$, χ^2-test) to 0.80±0.14% (n=1,119) from an index of 1.30±0.07% (n=2,225) in control brains, this reduction was associated with a small brain and disc phenotype (Fig. S1 in the supplementary material). TUNEL assays and labeling with antibody to caspase 3 showed that there was no detectable increase in apoptosis of cells in the *Chromator* mutant brains compared to wild type brains (data not shown) indicating that the smaller brain size was likely to be a result of attenuated cell proliferation caused by an inability of mutant cells to re-enter the cell cycle after failing to complete the previous one.

In order to verify that the observed defects were caused by impaired Chromator function we generated transgenic flies carrying full-length Chromator-GFP rescue constructs (NP-Chro) in the UASp vector under native promoter control as diagrammed in Fig. 2A. One construct contained wild type Chromator coding sequence and the other had a point mutation leading to a N^{41} to D^{41} amino acid change that abolished immunoreactivity to the NH_2-terminal Chromator mAb 12H9 (Rath et al., 2004; 2006). Expression of both constructs rescued the *Chromator* mutant phenotypes examined in this study including brain size (Fig. S1) and the coiled and condensed chromosome arm morphology of polytene chromosomes from $Chro^{71}/Chro^{612}$ mutant larvae (Fig. 2E). In addition, adult viability of $Chro^{71}/Chro^{612}$ mutants was restored to about 60% of wild type levels (data not shown) with both male and female flies being fertile. Immunoblot analysis showed that the NP-Chro protein in rescued flies of the $Chro^{71}/Chro^{612}$ mutant background was expressed at levels comparable to that of native Chromator in wild type flies (Fig. 2B). Importantly, NP-Chro showed normal localization to mitotic spindles in wild type syncytial embryos (Fig. 2D) as well as in $Chro^{71}/Chro^{612}$ mutant neuroblasts while rescuing spindle morphology (Fig. 2C) and significantly reducing the number of spindle defects by more than 70% ($p<0.001$, χ^2-test) to levels only twice that of wild type brains (Fig. 1C). In addition, we followed the localization and dynamic reorganization of NP-Chro during the cell cycle in live syncytial embyos using time-lapse confocal microscopy (Movie 1 in the supplementary material). The movie demonstrates the transition of

Chromator from its chromosomal localization at interphase to its spindle matrix and centrosomal localization at meta- and anaphase.

Chromator functions in at least two different molecular complexes, one comprising the spindle matrix at mitosis and one associated with nuclear and chromatin structure during interphase (Rath et al., 2004: 2006). Furthermore, deletion construct analysis in S2 cells showed that the chromodomain containing NH_2-terminal part of Chromator was not necessary for nuclear targeting or for localization to the spindle matrix (Rath et al., 2004). This suggests that the COOH-terminal part that includes the interaction domains for the spindle matrix proteins Skeletor and EAST may be responsible for targeting Chromator to the spindle matrix. To further explore this possibility we expressed three GFP-tagged pUAST or pUASP Chromator constructs containing different regions of the Chromator coding sequence transgenically in the *Chro*^{71}*/Chro*^{612} mutant background using a *elav-GAL4* driver line. The constructs are diagrammed in Fig. 3A and comprised a full-length construct (Chro-FL), a NH_2-terminal construct including the chromodomain (Chro-NTD), and a COOH-terminal construct (Chro-CTD). As illustrated by immunoblot analysis in Fig. 3B these constructs were expressed at relatively low levels compared to wild type Chromator and thus were not likely to have any dominant negative effects. However, even at these expression levels Chro-FL was able to significantly reduce the number of Chromator mutant spindle defects from 90.3% to 16.4% ($p<0.001$, χ^2-test) (Fig. 3C) which was similar to the reduction to 17.0% obtained by expressing NP-Chro (Fig. 1C). In contrast, there was no significant difference ($p>0.5$, χ^2-test) between the observed frequency of abnormal spindle phenotypes in Chromator mutants (90.3%) and in Chromator mutants expressing Chro-NTD (89.8%) (Fig. 3C). However, expression of Chro-CTD reduced spindle defects by about 40% (Fig. 3C), a significant reduction (($p<0.001$, χ^2-test) indicating that Chro-CTD at least had partial rescue function. Furthermore, both Chro-FL and Chro-CTD (Fig. 3D), but not Chro-NTD (Fig. 3D),

localized to the mitotic spindle apparatus confirming that the CTD-domain is sufficient for targeting of Chromator to the spindle matrix.

In order to further characterize the origin and cause of the chromosome segregation and spindle defects in the absence of Chromator function we performed time-lapse imaging analysis of mitosis in Chromator RNAi depleted live S2 cells. The S2 cells were stably co-expressing GFP-α-tubulin and the kinetochore marker mCherry-Centromere identifier (Cid) as previously described in Lince-Faria et al. (2009). In most Chromator RNAi treated cells a relatively normal bipolar microtubule spindle was formed and chomosomes congressed to the metaphase plate (Fig. 4C-E); however, in contrast to control cells (Fig. 4A, B) their alignment was incomplete as indicated by the displaced position of the mCherry-labeled kinetochores (Fig. 4C-E). For quantification of the maximal degree of chromosome alignment the metaphase plate was fitted with the smallest possible rectangle encompassing all of the kinetochores. Consequently, the width of this rectangle in μm represents a measure of the tightness and completeness of the kinetochore alignment. In Chromator RNAi-treated cells this width (2.96±0.82 μm, n=25) was significantly greater ($p<0.002$, Student's two-tailed t-test) than that observed in control cells (2.17±0.76 μm, n=23). Furthermore, as Chromator RNAi-treated S2 cells entered anaphase the microtubule spindle often frayed and/or split into multiple spindles with chromosomes scattered within the spindle (Fig. 4C, D; movie 4 and 5 in the supplementary material). That mitosis progresses into anaphase in Chromator RNAi-depleted cells despite misaligned chromosomes at the metaphase plate suggests a defective spindle assembly checkpoint (SAC). Recently, it was demonstrated by Lince-Faria et al. (2009) that the spindle matrix protein Megator is required for proper SAC response and recruitment of Mad2 to unattached kinetochores. For this reason we analyzed whether Mad2 localization was similarly affected after Chromator depletion by RNAi. As illustrated in Figs. 5A,B and 5D Mad2 kinetochore accumulation was significantly reduced in such cells as compared to control cells although immunoblot analysis showed that normal Mad2

expression levels were not affected by Chromator depletion (Fig. 5C). Furthermore, Chromator-depleted cells had a lower mitotic index as well as a weakened response to microtubule depolymerization (Fig. 5E) suggesting that like Megator, Chromator is required for proper SAC response.

An issue in interpreting the cause of the Chromator mutant spindle phenotypes is that Chromator at interphase affects chromatin structure (Rath et al., 2006) which could influence the expression of one or more genes thereby indirectly affecting the function of the spindle apparatus. During studies of potential interactions between Chromator and the kinesin 14 family motor protein Ncd we noted that Ncd protein levels were down-regulated in $Chro^{71}/Chro^{612}$ mutant backgrounds (Figs. 6A and 6B) whereas tubulin levels were relatively unaffected (Figs. 2B, 3B, and 6B). Moreover, Ncd protein levels were partially restored by expression of NP-Chro in the *Chromator* mutant background (Fig. 6B). The Ncd protein down-regulation either could be caused by increased protein turnover or by a reduction in transcription. To directly test whether transcription of *ncd* was affected by impaired Chromator function we used qRT-PCR to measure *ncd* mRNA transcript levels. Primers were designed that would amplify transcripts from the *ncd* gene, and primers specific to the gene encoding the ribosomal protein Rp49 were used for normalization as previously described (Cai et al., 2008). We performed several independent experiments in which total mRNA was isolated from wild type, $Chro^{71}/Chro^{612}$, and $JIL\text{-}1^{z2}/JIL\text{-}1^{z2}$ third instar larvae (Wang et al., 2001), and in which qRT-PCR determination of transcript levels was performed in duplicate. Determination of *ncd* transcript levels in the $JIL\text{-}1^{z2}/JIL\text{-}1^{z2}$ mutant background was included for comparison because *JIL-1* mutant polytene chromosomes have a similar phenotype to that observed in $Chro^{71}/Chro^{612}$ mutant larvae (Fig. 7A) (Rath et al., 2006). However, unlike in $Chro^{71}/Chro^{612}$ mutant neuroblasts spindle morphology in *JIL-1* mutant neuroblasts was essentially normal with only a moderate increase in the percentage of spindle defects (17.9%) over wild type (8.2%) in constrast to the 90.2% observed in the *Chromator* mutant background (Fig. 7B, C). As illustrated in Fig. 7C we found a significant decrease in *ncd* transcript

levels relative to *rp49* transcript levels in both $Chro^{71}/Chro^{612}$ and $JIL\text{-}1^{z2}/JIL\text{-}1^{z2}$ mutant larvae. Thus, these experiments indicate that transcript levels of some genes can be repressed in *Chromator* mutants as has also previously been observed in *JIL-1* mutant backgrounds (Lerach et al., 2005; Bao et al., 2007; Cai et al., 2008).

DISCUSSION

The co-localization and interactions of Chromator with the spindle matrix complex during mitosis (reviewed in Johansen and Johansen, 2007) suggests that Chromator may be involved in its function (Rath et al., 2004). A spindle matrix has been hypothesized to provide a stationary or elastic molecular matrix that can provide a substrate for motor molecules to interact with during microtubule sliding and which can stabilize the spindle during force production (Pickett-Heaps et al., 1997; Forer et al., 2008). Thus a prediction of the spindle matrix hypothesis is that if such a scaffold were interfered with, it would affect the assembly and/or dynamic behavior of the microtubule associated spindle apparatus and lead to abnormal chromosome segregation. In this study we have examined the phenotypic consequences of loss-of-function *Chromator* mutations on cell division in third instar larval brains. We show that mitotic neuroblasts from $Chro^{71}/Chro^{612}$ brain squash preparations have severe tubulin spindle and chromosome segregation defects that were associated with a reduction in brain size. The microtubule spindles at metaphase were incomplete, unfocused, and/or without clear spindle poles. At anaphase chromosomes were lagging and scattered indicating impaired spindle function, a phenotype similar to that previously obtained by Chromator RNAi depletion in S2 cells (Rath et al., 2004). Expression of full-length Chromator transgenes under endogenous promoter control partly or completely restored both viability, microtubule spindle morphology, as well as brain size strongly indicating that the observed mutant defects were directly attributable to lack of Chromator function. Thus, these data provide evidence that Chromator is a nuclear derived protein that plays a role in proper spindle dynamics leading to chromosome separation during mitosis.

In previous studies RNAi depletion of the spindle matrix proteins Skeletor, Megator, and EAST in S2 cells did not reveal any obvious microtubule spindle or chomosome segregation defects (Rath et al., 2004; Qi et al., 2004; H. Qi unpublished observations). However, recently using live imaging of Megator RNAi depleted S2 cells, Lince-Faria et al. (2009) showed that

Megator and its human ortholog Tpr function as spatial regulators of the spindle assembly checkpoint that ensures the efficient recruitment of Mad2 and Mps1 to unattached kinetochores at the onset of mitosis for proper spindle maturation. Here we provide evidence that Mad2 localization was similarly affected after Chromator depletion by RNAi and that Chromator-depleted cells had a lower mitotic index, suggesting that Chromator, like Megator, is required for proper SAC response.

The observed Chromator mutant phenotypes could be arrived at in a number of ways. For example, they could be caused by incomplete microtubule spindle formation and failure of the chromosomes to congress. However, time-lapse analysis of mitosis in Chromator RNAi depleted S2 cells suggested that bipolar microtubule spindle formation was relatively normal and that chromosomes congressed to the metaphase plate. However, in most cases their alignment was incomplete and as anaphase commenced the microtubule spindle often frayed and became unstable resulting in lagging and scattered chromosomes. These observations are compatible with the hypothesis that Chromator may constitute a functional component of a spindle matrix molecular complex that serves to stabilize the microtubule spindle apparatus during anaphase and is necessary for proper chromosome segregation.

A potential caveat to the interpretation of loss-of-function Chromator phenotypes is that Chromator is known to participate in at least two different molecular complexes, one of which is associated with nuclear and chromatin structure during interphase (Rath et al., 2004; 2006). Thus, loss-of-function mutations in the Chromator gene in addition to directly affecting mitosis may also influence the expression of other genes due to perturbations of their chromatin environment thereby potentially indirectly affecting the function of the microtubule based spindle apparatus. Using immunoblot analysis we found that the level of at least one such protein Ncd was reduced by 80% in *Chromator* loss-of-function mutants. qRT-PCR determination showed that this reduction was likely to have been caused by repressed transcription rather than by increased protein turnover. However, the finding that tubulin levels in the *Chromator* mutant background as

well as Mad2 levels in Chromator RNAi-depleted S2 cell were relatively unaffected suggests that lack of Chromator does not cause a general repression of all genes. Interestingly, in mutant larvae lacking the histone H3S10 kinase JIL-1 which has a similar chromatin phenotype to that of *Chro*^{71}*/Chro*^{612} mutants *ncd* mRNA levels were also reduced. However, in *JIL-1* null mutant brains mitosis was close to normal with only a moderate increase in the percentage of spindle and chromosome segregation defects compared to wild type in spite of the perturbed chromosome morphology. While reduced levels of Ncd by RNAi treatment in S2 cells results in clear spindle defects (Goshima and Vale, 2003) this phenotype is very different from the *Drosophila ncd* null mutant, in which meiotic spindle defects are observed, but where spindle formation defects in mitotic cells are very subtle or absent (Endow et al., 1994; Goshima and Vale, 2003). Thus, the downregulation of Ncd in the *Chromator* mutant background is unlikely to account for the majority of the mitotic defects observed in the larval neuroblasts. However, it remains a possibility that other unknown genes involved in mitosis may be repressed as well. To determine the genes whose expression is affected by the chromatin perturbation induced by lack of Chromator will require a future genome-wide survey. Consequently, at present it is not possible to unequivocally link the phenotypes observed in this study with Chromator's function as a spindle matrix member. Nonetheless, that Chromator function, whether directly or indirectly, is required for proper microtubule spindle formation and mitosis was demonstrated by the rescue of mutant phenotypes by transgenic expression of Chromator-GFP.

ACKNOWLEDGMENTS

We thank members of the laboratory for discussion, advice, and critical reading of the manuscript. We also wish to acknowledge Ms. V. Lephart for maintenance of fly stocks and Mr. Laurence Woodruff for technical assistance. We especially thank Dr. S. Endow for providing the Ncd antibody. Work in the laboratory of J.J. and K.M.J. is supported by NSF grant MCB0817107. Work in the lab. of H.M. is supported by grants PTDC/BIA-BCM/66106/2006 and PTDC/SAU-OBD/66113/2006 from FCT, the Gulbenkian Programmes for Research Stimulation and Frontiers in the Life Sciences and the Luso-American Foundation for Development/National Science Foundation Research Network.

REFERENCES

Bao, X., Deng, H., Johansen, J., Girton, J. and Johansen, K.M. 2007. Loss-of-function alleles of the JIL-1 histone H3S10 kinase enhance position-effect-variegation at pericentric sites in *Drosophila* heterochromatin. Genetics 176, 1355-1358.

Bonaccorsi, S., Giansanti, M.G. and Gatti, M. 2000. Spindle assembly in *Drosophila* neuroblasts and ganglion mother cells. Nat. Cell Biol. 2, 54-6.

Brand A.H., and Perrimon, N. 1993. Targeted gene expression as a means of altering cell fates and generating dominant phenotypes. Development. 118, 401-15.

Cai, W., Bao, X., Deng, H., Jin, Y., Girton, J., Johansen, J. and Johansen, K.M. 2008. RNA polymerase II-mediated transcription at active loci does not require histone H3S10 phosphorylation in *Drosophila*. Development 135, 2917-2925.

Endow, S.A., Chandra, R., Komma, D.J., Yamamoto, A.H. and Salmon, E.D. 1994. Mutants of the *Drosophila* ncd microtubule motor protein cause centrosomal and spindle pole defects in mitosis. J. Cell Sci. 107, 859-867.

Forer, A., Pickett-Heaps, J.D., and Spurk, T. 2008. What generates flux of tubulin in kinetochore microtubules? Protoplasma 232, 137-141.

Gortchakov, A.A., Eggert, H., Gan, M., Mattow, J., Zhimulev, I.F. and Saumweber, H. 2005. Chriz, a chromodomain protein specific for the interbands of *Drosophila melanogaster* polytene chromosomes. Chromosoma 114, 54-66.

Goshima, G. and Vale, R.D. 2003. The roles of microtubule-based motor proteins in mitosis: comprehensive RNAi analysis in the *Drosophila* S2 cell line. J. Cell Biol. 162, 1003-1016.

Jin, Y., Wang, Y., Walker, D. L, Dong, H., Conley, C., Johansen, J. and Johansen, K.M. 1999. JIL-1: a novel chromosomal tandem kinase implicated in transcriptional regulation in Drosophila. Mol. Cell 4, 129-135.

Johansen, K.M., and Johansen, J. 2003. Studying nuclear organization in embryos using antibody tools. In: *Drosophila* Cytogenetics Protocols, ed. D.S. Henderson, Totowa, NJ: Humana Press, p. 215-234.

Johansen, K.M. and Johansen, J. 2007. Cell and molecular biology of the spindle matrix. Int. Rev. Cytol. 263, 155-206.

Kelley, R. L., Meller, V. H., Gordadze, P. R., Roman, G., Davis, R. L. and Kuroda, M. I. 1999. Epigenetic spreading of the *Drosophila* dosage compensation complex from roX RNA genes into flanking chromatin. Cell 98, 513-522.

Lerach, S., Zhang, W., Deng, H., Bao, X., Girton, J., Johansen, J., and Johansen, K.M. 2005. JIL-

1 kinase, a member of the male-specific lethal (MSL) complex, is necessary for proper dosage compensation of eye pigmentation in *Drosophila*. Genesis 43, 213-215.

Lindsley, D. L. and Zimm, G. G. (1992). The genome of *Drosophila melanogaster*. Academic Press, New York. 1133 pp.

Linse-Faria, M., Maffini, S., Orr, B., Ding, Y., Florindo, C., Sunkel, C.E., Tavares, A., Johansen, J., Johansen, K.M. and Maiato, T. 2009. Spatiotemporal control of mitosis by the conserved spindle matrix protein Megator. J. Cell. Biol. 184, 647-657.

Maiato, H., Hergert, P.J., Moutinho-Pereira, S., Dong, Y., Vandenbeldt, K.J., Rieder, C.L. and McEwen, B.F. 2006. The ultrastructure of the kinetochore and kinetochore fiber in Drosophila somatic cells. Chromosoma 115, 469-80.

Mendjan, S., Taipale, M., Kind, J., Holz, H., Gebhardt, P., Schelder, M., Vermeulen, M., Buscaino, A., Duncan, K., Mueller, J., Wilm, M., Stunnenberg, H.G., Saumweber, H., and Akhtar, A. 2006. Nuclear pore components are involved in the transcriptional regulation of dosage comesation in *Drosophila*. Mol. Cell 21, 811-823.

Pickett-Heaps, J. D., Forer, A., and Spurck, T. 1997. Traction fibre: toward a "tensegral" modle of the spindle. Cell Motil. Cytoskel. 37, 1-6.

Qi, H., Rath, U., Wang, D., Xu, Y.-Z., Ding, Y., Zhang, W., Blacketer, M., Paddy, M., Girton, J., Johansen J., and Johansen, K.M. 2004. Megator, an essential coiled-coil protein localizes to the putative spindle matrix during mitosis. Mol. Biol. Cell 15, 4854-4865.

Qi, H., Rath, U., Ding, Y., Ji, Y., Blacketer, M. J., Girton, J., Johansen, J., and Johansen, K.M. 2005. EAST interacts with Megator and localizes to the putative spindle matrix during mitosis in Drosophila. J. Cell Biochem. 95, 1284-1291.

Rath, U., Wang, D., Ding, Y., Xu, Y.-Z., Qi, H., Blacketer, M.J., Girton, J., Johansen, J. and Johansen, K.M. 2004. Chromator, a novel and essential chromodomain protein interacts directly with the putative spindle matrix protein Skeletor. J. Cell. Biochem. 93, 1033-1047.

Rath, U., Ding, Y., Deng, H., Qi, H., Bao, X., Zhang, W., Girton, J., Johansen, J., and Johansen, K. M. 2006. The chromodomain protein, Chromator, interacts with JIL-1 kinase and regulates the structure of *Drosophila* polytene chromosomes. J. Cell Sci. 119, 2332-2341.

Roberts, D.B. 1998. In *Drosophila*: A Practical Approach. IRL Press, Oxford, UK. 389 pp.

Rorth, P. 1998. Gal4 in the *Drosophila* female germline. Mech. Dev. 78,113-8.

Sambrook, J. and Russell, D.W. 2001. Molecular Cloning: A Laboratory Manual. (Cold Spring Harbor Laboratory Press, NY).

Towbin, H., Staehelin, T. and Gordon, J. 1979. Electrophoretic transfer of proteins from polyacrylamide gels to nitrocellulose sheets: Procedure and some applications. Proc. Natl. Acad. Sci. USA 9, 4350-4354.

Walker, D.L., Wang, D., Jin, Y., Rath, U., Wang, Y., Johansen, J. and Johansen, K.M. 2000. Skeletor, a novel chromosomal protein that redistributes during mitosis provides evidence for the formation of a spindle matrix. J. Cell Biol. 151, 1401-1411.

Wang, Y., Zhang, W., Jin, Y., Johansen, J. and Johansen, K.M. 2001. The JIL-1 tandem kinase mediates histone H3 phosphorylation and is required for maintenance of chromatin structure in Drosophila. Cell 105, 433-443.

Wasser, M., Osman, Z.B., and Chia, W. 2007. EAST and Chromator control the destruction and remodeling of muscles during Drosophila metamorphosis. Dev. Biol. 307, 380-393.

Zhang, W., Jin, Y., Ji, Y., Girton, J., Johansen, J. and Johansen, K.M. 2003. Genetic and phenotypic analysis of alleles of the Drosophila chromosomal JIL-1 kinase reveals a functional requirement at multiple developmental stages. Genetics 165, 1341-1354.

FIGURE LEGENDS

Fig. 1. Spindle defects in *Chromator* mutant neuroblasts. Neuroblasts from third instar larval brain squashes of control brains (A1-3) and of $Chro^{71}/Chro^{612}$ *Chromator* mutant brains (B1-6) double labeled with tubulin antibody (red) and histone H3S10ph antibody (green). B1-6 shows examples of misaligned and incomplete spindles in *Chromator* mutant neuroblasts at meta- and anaphase. Scale bar for the images in (A) and (B) equals 5 μm. (C) Histograms of the percentage of mitotic cells in larval brains with spindle defects in wild type, in $Chro^{71}/Chro^{612}$ mutants, and in $Chro^{71}/Chro^{612}$ mutants expressing a full-length Chromator-GFP rescue construct (NP-Chro) under endogenous promoter control. The difference in the frequency of mitotic phenotypes in neuroblasts in the $Chro^{71}/Chro^{612}$ mutant background was significantly different from that observed in both wild-type and $Chro^{71}/Chro^{612}$ mutants expressing the NP-Chro transgene ($p<0.001$, χ^2-test). However, full rescue was not attained as there still was a significant difference between $Chro^{71}/Chro^{612}$ mutants expressing the NP-Chro construct and wild type ($p<0.01$, χ^2-test). The total number of mitotic neuroblasts examined is indicated at the bottom of the histograms.

Fig. 2. Transgenic expression of full-length Chromator-GFP. (A) Diagram of the NP-Chro rescue construct. *Chromator* exons are shown in red, the upstream regulatory region is in yellow, a small stretch included of the coding sequence for the neighboring *Ssl1* gene is in blue, and the GFP tag is in green. (B) Immunoblot of protein extracts from larval brains from wild type (wt), *Chromator* mutants ($Chro^{71}/Chro^{612}$), and *Chromator* mutants expressing NP-Chro (NP-Chro, $Chro^{71}/Chro^{612}$) labeled with GFP pAb and the Chromator mAb 6H11. Labeling with tubulin antibody was used as a loading control. The relative migration of molecular size markers is indicated to the left in kD. (C) Mitotic neuroblast at metaphase from a $Chro^{71}/Chro^{612}$ mutant larvae expressing the NP-Chro construct. NP-Chro was labeled with GFP antibody (in green),

tubulin with anti-tubulin antibody (in red), and DNA with Hoechst (in grey/blue). Scale bar equals 5 μm. (D) Mitotic spindles at metaphase from a wild type syncytial embryo expressing the NP-Chro construct. NP-Chro was labeled with GFP antibody (in green), tubulin with anti-tubulin antibody (in red), and DNA with Hoechst (in grey/blue). Scale bar equals 10 μm. (E) Polytene squash preparations from *Chromator* mutant (*Chro*^{71}/*Chro*^{61}) larvae with (lower panel) or without (upper panel) expression of the NP-Chro rescue construct. NP-Chro was labeled with Chromator mAb 6H11 (in red) and DNA with Hoechst (in blue/grey). mAb 6H11 does not recognize the truncated mutant proteins generated by the *Chro*^{71} and *Chro*^{612} alleles. Scale bar equals 20 μm.

Fig. 3. Expression of Chromator deletion constructs transgenically in a *Chro*^{71}/*Chro*^{612} mutant background. (A) Diagrams of the Chromator GFP tagged constructs analyzed. The chromodomain region is shown in black and the position of the GFP tag in green. (B) Immunoblot of protein extracts from larval brains from wild type (wt), *Chromator* mutants (*Chro*^{71}/*Chro*^{612}), and *Chromator* mutants expressing either Chro-FL, Chro-NTD, or Chro-CTD using the brain specific *GAL4-elav* driver labeled with the C-terminal Chromator mAb 6H11 and the N-terminal Chromator mAb 12H9, respectively. Labeling with tubulin antibody was used as a loading control. The relative migration of molecular size markers is indicated to the left in kD. (C) Histograms of the percentage of mitotic cells in larval brains with spindle defects in wild type, in *Chro*^{71}/*Chro*^{612} mutants, and in *Chro*^{71}/*Chro*^{612} mutants expressing Chro-FL, Chro-CTD, or Chro-NTD using the *GAL4-elav* driver. The difference in the frequency of mitotic phenotypes in neuroblasts in the *Chro*^{71}/*Chro*^{612} mutant background was significantly different from that observed in *Chro*^{71}/*Chro*^{612} mutants expressing the Chro-FL or Chro-CTD transgenes ($p<0.001$, χ^2-test) but not from that observed in *Chro*^{71}/*Chro*^{612} mutants expressing the Chro-NTD transgene ($p>0.5$, χ^2-test). In addition, all three transgenic lines were significantly different from wild type (Chro-FL, $p<0.01$; Chro-CTD, $p<0.001$; Chro-NTD, $p<0.001$; χ^2-tests). The total number of mitotic

neuroblasts examined is indicated at the bottom of the histograms. (D) Mitotic neuroblasts from *Chro*^{71}*/Chro*^{612} mutant larvae expressing Chro-FL (upper panel) and Chro-CTD (middle panel) as well as a mitotic neuroblast from a wild type larvae expressing Chro-NTD (lower panel). Chro-FL, Chro-CTD, and Chro-NTD were labeled with GFP antibody (in green), tubulin with anti-tubulin antibody (in red), and DNA with Hoechst (blue in the composite). Scale bar equals 5 μm.

Fig. 4. Mitotic spindle and chromosome segregation defects observed in time-lapse movies of control and Chromator RNAi depleted S2 cells. (A, B) Control cells stably co-expressing GFP-α-tubulin (in green) and mCherry-Cid (in red). (C-E) Chromator RNAi depleted S2 cells stably co-expressing GFP-α-tubulin (in green) and mCherry-Cid (in red). The first frame shows kinetochore positioning at the time of maximal alignment at the metaphase plate and the time elapsed from this timepoint is indicated in minutes for the subsequent frames. Scale bar equals 5 μm. The complete movies from which the images shown were derived are included in the online supplementary material as movie 2-6.

Fig. 5. Mad2 requires Chromator to localize to unattached kinetochores. (A-D) S2 cells treated with colchicine and processed for immunofluorescence with Mad2 (red) and Cid (Green) antibodies. DNA (blue) was counterstained with DAPI. (A) Control, (B) Chromator RNAi. The scale bar equals 5 μm. (C) Immunoblot analysis of protein extracts from control (lane 1) and Chromator RNAi-treated (lane 2) S2 cells labeled with antibodies to Chromator, tubulin, and Mad2. (D) Quantification of Mad2/CID pixel intensity at kinetochores for control (n=224 kinetochores, 14 cells) and Chromator RNAi (n=251 kinetochores, 16 cells). The two populations are statistically different ($p<0.001$; Mann-Whitney test). (E) Mitotic index under physiological conditions and after colchicine treatment. Error bars represent standard deviation from the mean from three independent experiments.

Fig. 6. Expression of the microtubule based motor protein Ncd is attenuated in the *Chro*^{71}*/Chro*^{612} mutant background. (A) Mitotic neuroblasts at metaphase from witd type (wt) and *Chro*^{71}*/Chro*^{612} mutant larvae. Ncd was labeled with anti-Ncd antibody (in green), tubulin with anti-tubulin antibody (in red), and DNA with Hoechst (blue in the composite). Scale bar equals 5 μm. (B) Immunoblot of protein extracts from larval brains from wild type (wt), *Chromator* mutants (*Chro*^{71}*/Chro*^{612}), and *Chromator* mutants expressing NP-Chro (NP-Chro, *Chro*^{71}*/Chro*^{612}) labeled with the Chromator mAb 6H11 (upper panel) and with Ncd antibody (middle panel). Labeling with tubulin antibody was used as a loading control (lower panel). (C) Transcript levels of *ncd* mRNA in wild type (wt), *Chromator* mutant (*Chro*^{71}*/Chro*^{612}), and *JIL-1* null mutant backgrounds. *ncd* transcript levels were determined by qRT-PCR and normalized to the mRNA levels of Ribosomal protein 49 (RP49). Each determination was performed in duplicate and error bars indicate the s.d.m.

Fig. 7. Comparison of chromosome and spindle defects in *Chromator* and *JIL-1* mutant backgrounds. (A) Polytene chromsome squash preparations from wild type, *Chromator* mutant (*Chro*^{71}*/Chro*^{612}), and *JIL-1* mutant (*JIL-1*^{z2}*/JIL-1*^{z2}) larvae labeled with Hoechst. Scale bar equals 20 μm. (B) Neuroblasts from third instar larval brain squashes of *JIL-1* mutant (*JIL-1*^{z2}*/JIL-1*^{z2}) brains double labeled with tubulin antibody (red) and histone H3S10ph antibody (green). Scale bar equals 2 μm. (C) Histograms of the percentage of mitotic cells in larval brains with spindle defects in wild type as well as in *Chromator* (*Chro*^{71}*/Chro*^{612}) and *JIL-1* (*JIL-1*^{z2}*/JIL-1*^{z2}) mutant brains. The difference in the frequency of mitotic phenotypes in neuroblasts in the *Chro*^{71}*/Chro*^{612} mutant background was significantly different from that observed in both wild-type and *JIL-1*^{z2}*/JIL-1*^{z2} mutants ($p<0.001$, χ^2-test). The total number of mitotic neuroblasts examined is indicated at the bottom of the histograms.

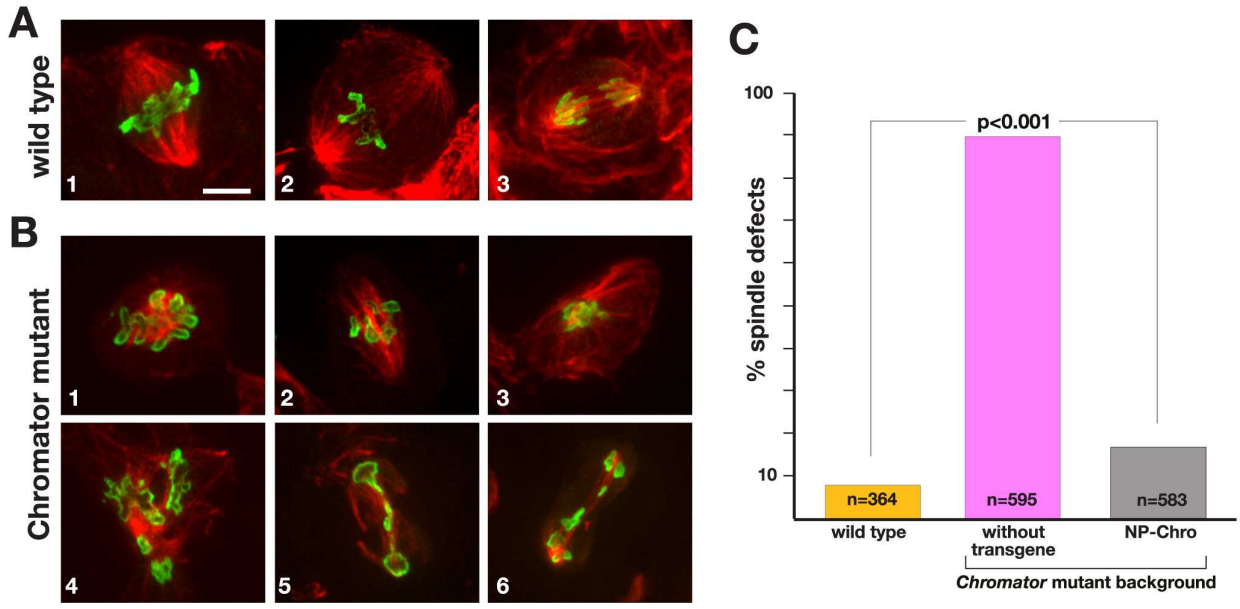
A
wild type
1
2
3
B
Chromator mutant
1
2
3
4
5
6
C
100
10
% spindle defects
p<0.001
n=364
n=595
n=583
wild type
without transgene
NP-Chro
Chromator mutant background

Fig. 1

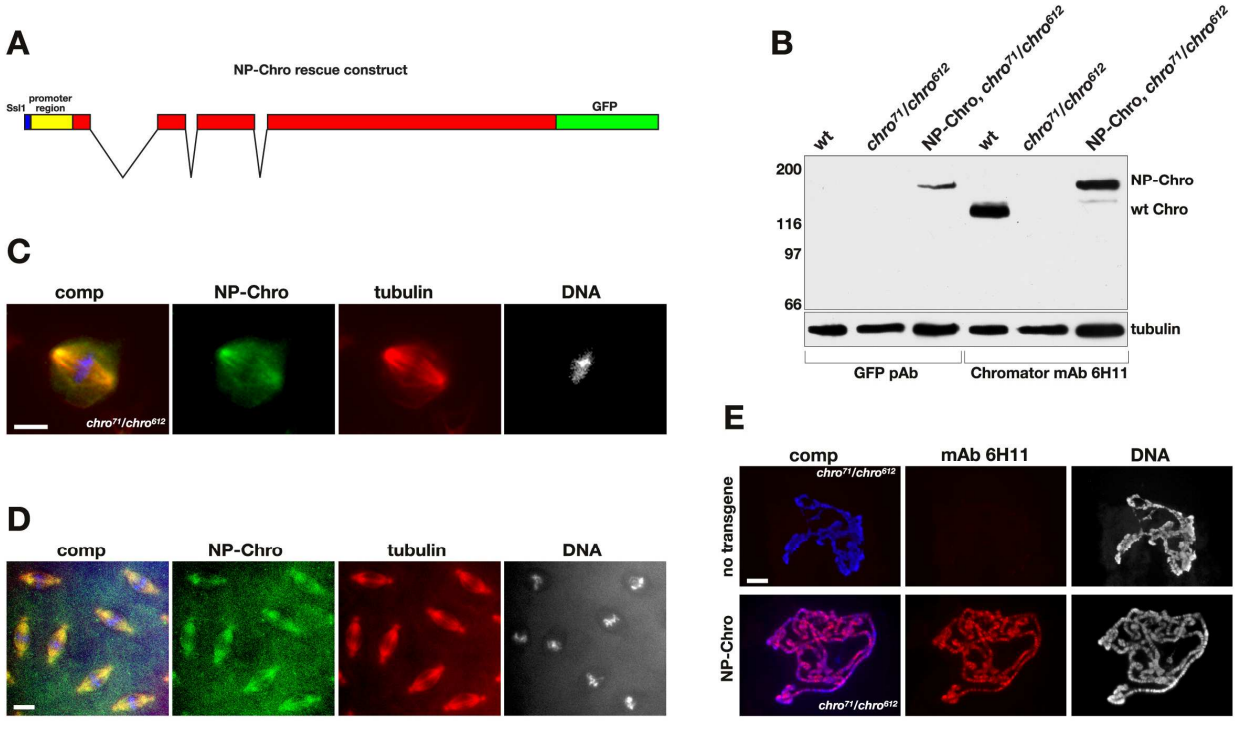
A
NP-Chro rescue construct
Ssh1
promoter region
GFP
B
wt
chro71/chro612
NP-Chro, chro71/chro612
wt
chro71/chro612
NP-Chro, chro71/chro612
200
116
97
66
NP-Chro
wt Chro
tubulin
GFP pAb
Chromator mAb 6H11
C
comp
NP-Chro
tubulin
DNA
chro71/chro612
D
comp
NP-Chro
tubulin
DNA
E
comp
mAb 6H11
DNA
no transgene
NP-Chro
chro71/chro612
chro71/chro612

Fig. 2

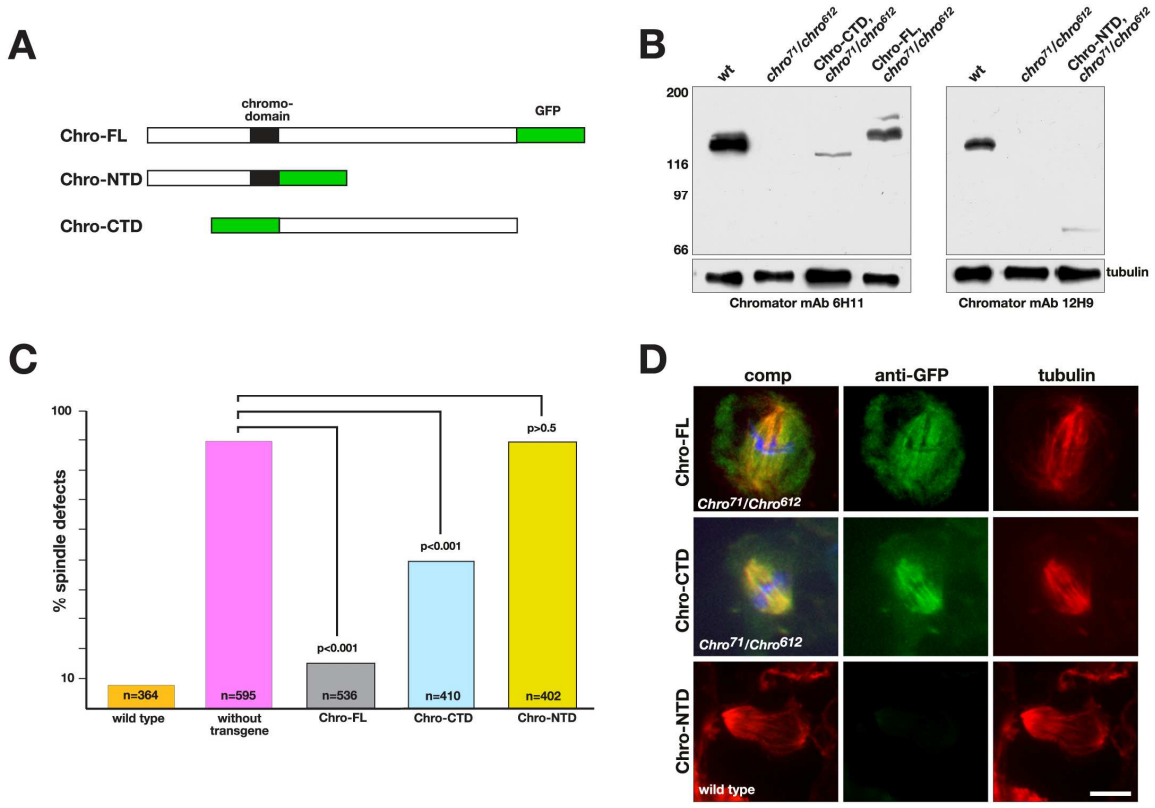
A
chromo-domain
GFP
Chro-FL
Chro-NTD
Chro-CTD
B
wt
chro71/chro612
Chro-CTD, chro71/chro612
Chro-FL, chro71/chro612
Chro-NTD, chro71/chro612
200
116
97
66
tubulin
Chromator mAb 6H11
Chromator mAb 12H9
C
% spindle defects
100
10
p>0.5
p<0.001
p<0.001
n=364
n=595
n=536
n=410
n=402
wild type
without transgene
Chro-FL
Chro-CTD
Chro-NTD
D
comp
anti-GFP
tubulin
Chro-FL
Chro-CTD
Chro-NTD
Chro71/Chro612
Chro71/Chro612
wild type

Fig. 3

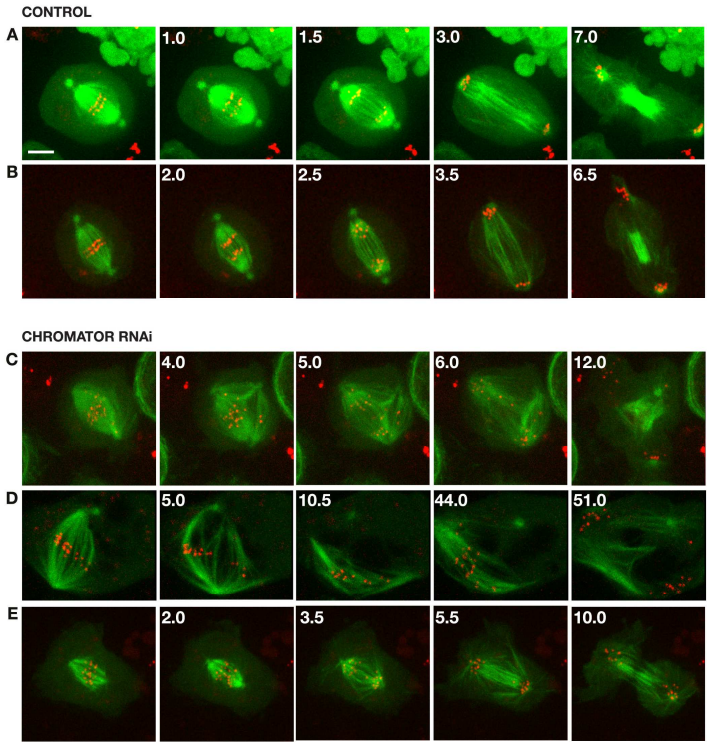
CONTROL
A
1.0
1.5
3.0
7.0
B
2.0
2.5
3.5
6.5
CHROMATOR RNAi
C
4.0
5.0
6.0
12.0
D
5.0
10.5
44.0
51.0
E
2.0
3.5
5.5
10.0

Fig. 4

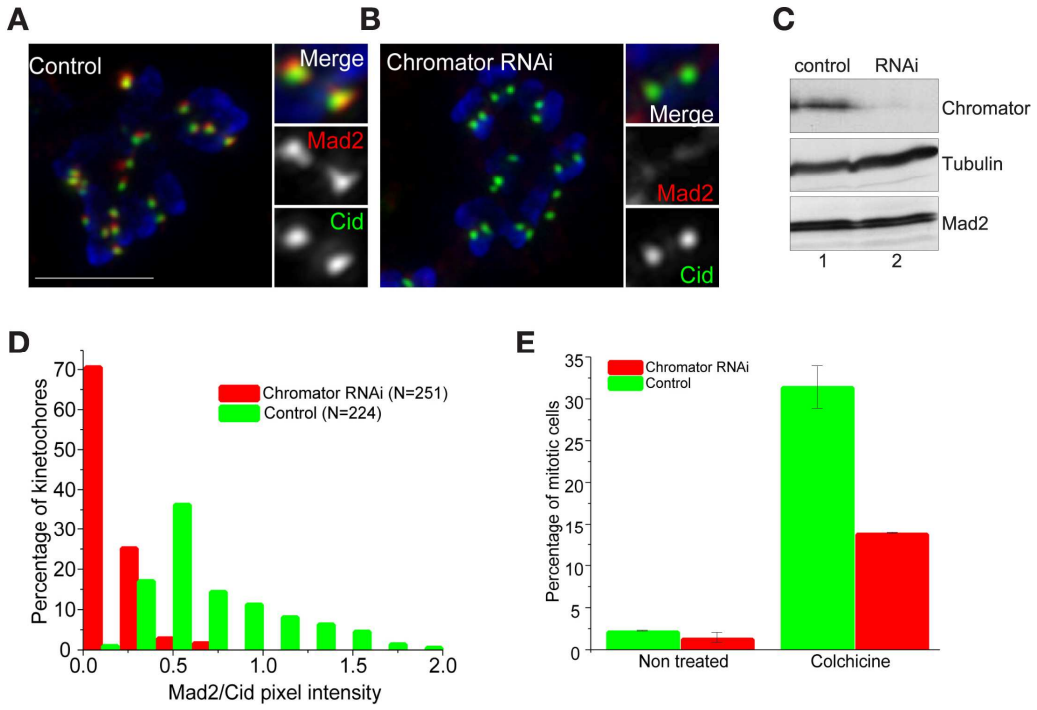
A
Control
Merge
Mad2
Cid
B
Chromator RNAi
Merge
Mad2
Cid
C
control
RNAi
Chromator
Tubulin
Mad2
1
2
D
Percentage of kinetochores
Chromator RNAi (N=251)
Control (N=224)
Mad2/Cid pixel intensity
E
Percentage of mitotic cells
Chromator RNAi
Control
Non treated
Colchicine

Fig. 5

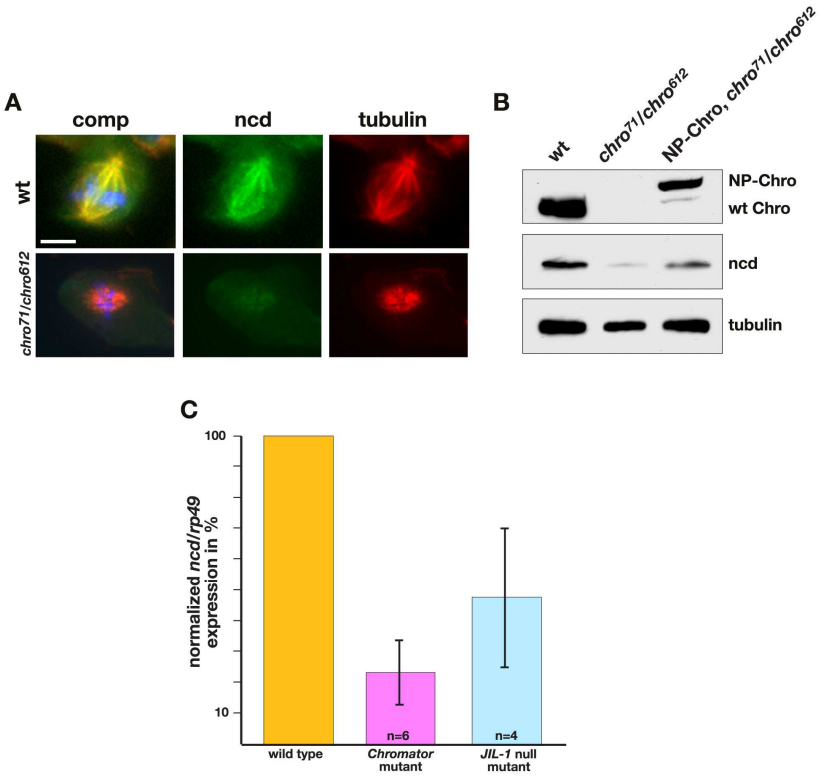
A
comp
ncd
tubulin
wt
chro71/chro612
B
wt
chro71/chro612
NP-Chro, chro71/chro612
NP-Chro
wt Chro
ncd
tubulin
C
normalized ncd/rp49 expression in %
wild type
Chromator mutant
JIL-1 null mutant
n=6
n=4

Fig. 6

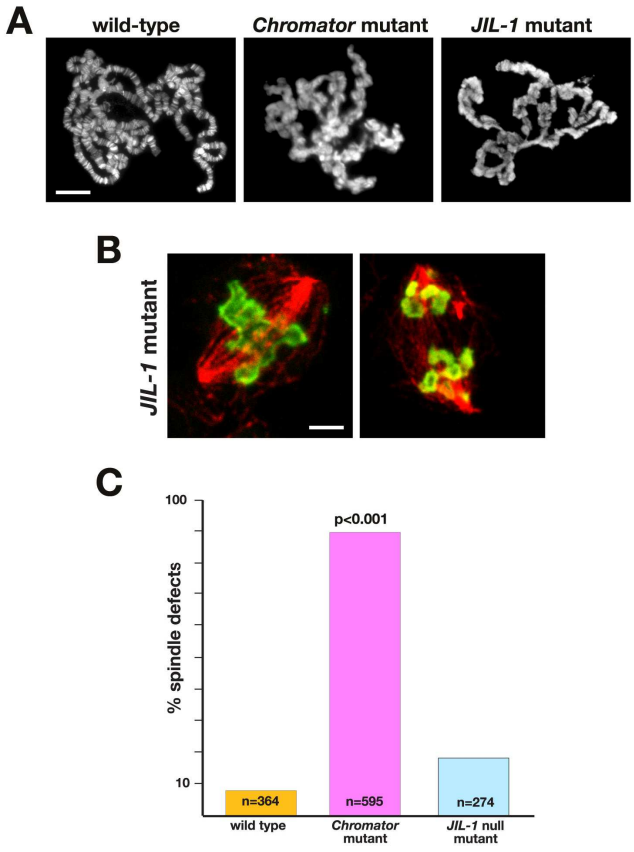
A
wild-type
Chromator mutant
JIL-1 mutant
B
JIL-1 mutant
C
100
10
% spindle defects
p<0.001
n=364
n=595
n=274
wild type
Chromator mutant
JIL-1 null mutant

Fig. 7

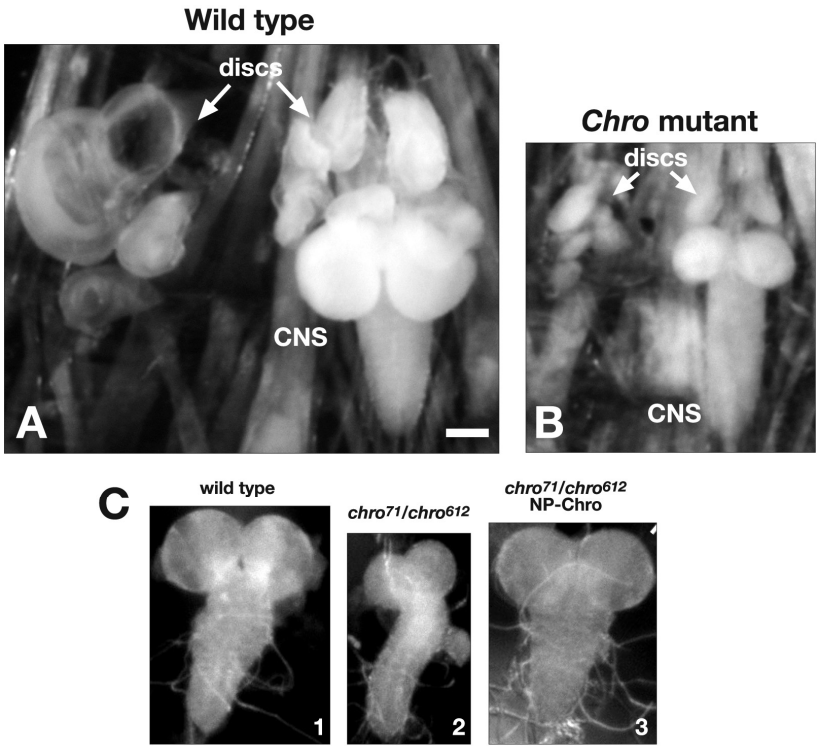
Wild type
discs
CNS
A
Chro mutant
discs
CNS
B
C
wild type
chro71/chro612
chro71/chro612
NP-Chro
1
2
3

Figure S1.